# Photo-Induced Dipoles: A New Method to Convert Photons into Photovoltage in Quantum Dot Sensitized Solar Cells

**ARTICLE** *in* NANO LETTERS · AUGUST 2013

Impact Factor: 13.59 · DOI: 10.1021/nl402360f · Source: PubMed



**5 AUTHORS**, INCLUDING:

Idan Hod
Northwestern University
**26** PUBLICATIONS **1,008** CITATIONS
SEE PROFILE

Arie Zaban
Bar Ilan University
**167** PUBLICATIONS **10,549** CITATIONS
SEE PROFILE

NANO LETTERS

Letter

pubs.acs.org/NanoLett

# Photo-Induced Dipoles: A New Method to Convert Photons into Photovoltage in Quantum Dot Sensitized Solar Cells

Sophia Buhbut,[†,§] Stella Itzhakov,[‡,§] Idan Hod,[†] Dan Oron,[‡] and Arie Zaban*[,†]

[†]Deparment of Chemistry, Bar Ilan University, Ramat-Gan, 52900, Israel

[‡]Department of Physics of Complex Systems, Weizmann Institute of Science, Rehovot 76100, Israel

Supporting Information

**ABSTRACT:** A high photovoltage is an essential ingredient for the construction of a high-efficiency quantum dot sensitized solar cell (QDSSC). In this paper we present a novel configuration of QDSSC which incorporates the photoinduced dipole (PID) phenomenon for improved open circuit voltage ($V_{oc}$). This configuration, unlike previously studied ones with molecular dipoles, is based on a dipole moment which is created only under illumination and is a result of exciton dissociation. The generation of photodipoles was achieved by the creation of long-lived trapped holes inside a core of type-II ZnSe/CdS colloidal core/shell QDs, which are placed on top of the standard CdS QD sensitizer layer. Upon photoexcitation, the created photodipole negatively shifts the $TiO_2$ energy bands, resulting in a photovoltage that is higher by ~100 mV compared to the standard cell, without type-II QDs. The extra photovoltage gained diminishes the excessive overpotential losses caused by the energetic difference between the CdS sensitizer layer and the $TiO_2$, without harming the charge injection processes. Moreover, we show that the extent of the additional photovoltage is controlled by the illumination intensity. This work provides new understanding regarding the operation mechanisms of photoelectrochemical cells, while presenting a new strategy for constructing a high-voltage QDSSCs. In addition, the PID effect has the potential to be implemented in other promising photovoltaic technologies.

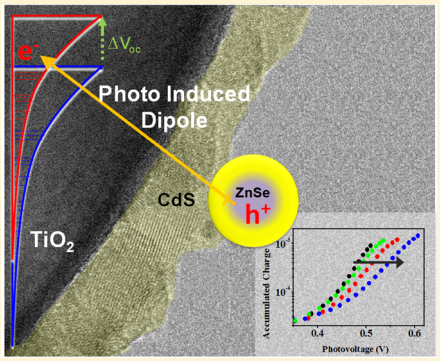


**KEYWORDS:** *Solar energy, quantum dot sensitized solar cell, dipole moment, high photovoltage cell, type-II QDs*

Nanomaterials, such as semiconductor nanocrystals (quantum dots, QDs), offer new approaches to efficient photo excitation and charge separation in photovoltaic (PV) devices.[1−5] The combination of novel nanoscale properties with low cost processability can potentially improve the energy conversion efficiency of a PV cell and decrease its production cost. In recent years, QDs have emerged as a promising alternative for the organic absorber in dye sensitized solar cells (DSSCs) due to their relatively high absorption cross section and control of the absorption onset wavelength using the quantum confinement effect.[6−18] The operation of QD sensitized solar cells (QDSSCs) is, in its most general aspects, similar to the well-known DSSC.[19] Under illumination, photons are absorbed by the QDs, which inject the excited electrons into a wide bandgap semiconductor electrode while holes are transferred via a liquid electrolyte or a solid hole conductor to the back electrode.

In the past few years, a rapid increase in the efficiencies obtained from QDSSCs has been reported, reaching values of around 6% (for CdSe QDs).[20−25] While these values still lag behind those of DSSCs, a further performance improvement for QDSSCs can be anticipated.

Recently, Park and coauthors have introduced the possibility of using a doped near IR PbS sensitizer to obtain extremely high photocurrents of about 30 mA.[23] Consequently, to date the main obstacle that needs to be solved in order to dramatically improve the conversion efficiencies of QDSSCs is the intrinsically low photovoltage obtained due to the highly negative redox potential of the commonly used polysulfide electrolyte. Several attempts have been made to overcome this limitation. For instance, high-voltage devices can be obtained by replacing the conventional polysulfide electrolyte with alternative mediator with more positive redox potential.[6,26] These alternatives can be either redox couples, such as the cobalt-based one, or solid-state hole conductors, like spiro-OMeTAD, P3HT that in addition avoids the use of volatile liquids.[24,27−31]

An additional route for improving the photovoltage in photoelectrochemical solar cells involves the use of molecular dipoles. In hybrid systems, organic molecules adsorbed on the surface of an inorganic semiconductor can modify its electronic properties, such as band bending, electron affinity, and work function, according to the needs of organic electronic devices.[32−35] For DSSCs, control of the band alignment was demonstrated via the use of molecular coadsorbents, leading to charge accumulation in the anode.[36] An additional study has shown the possibility to vary, the $V_{oc}$ of DSSCs, using the dipole moment of acid derivatives coadsorbed on the $TiO_2$

**Received:** June 27, 2013
**Revised:** August 6, 2013
**Published:** August 13, 2013

   dx.doi.org/10.1021/nl402360f | *Nano Lett.* 2013, 13, 4456−4461

surface.[37] In our previous work, we have demonstrated a systematic shift of QD energy levels with respect to an adjacent semiconductor using molecular dipoles that serve as a band alignment control tool for QDSSCs.[38−40] However, the effect of dipole molecules on the energy level alignment in those cells was relatively small because the resulting dipole moments were based only on partial charges.

Recently it has been shown that QDs in QDSSC can build up a chemical potential, which is attributed to charge accumulation in surface trap states.[41,42] This means that QDs, in addition to the wide band gap semiconductor (such as $TiO_2$ or ZnO), can also contribute to the total chemical capacitance in QDSSC. Knowing that, we were interested to find out whether in certain cases charges trapped in the QDs can also create an electrostatic charging effect. If such a phenomenon exists, there should be a possibility to utilize electrostatic dipoles that are based on transfer of whole charges in order to significantly manipulate the energy level alignment of the system while gaining extra photovoltage. A natural realization of this idea is via the use of multilayer QD organization, which has already proven beneficial in various QDSSC architectures.[43]

Here, we propose a strategy that will open a new path for the fabrication of highly efficient QDSSCs by using a photoinduced dipole (PID) phenomenon for which a capacitor-like device is created upon illumination. This concept is realized by depositing colloidal QDs with an engineered energy band alignment on top of the standard sensitizer layer to construct a PID cell. These QDs have a type-II core/shell structure in which the exciton readily dissociates, that is, the electron and the hole are confined to the shell and the core, respectively.[44,45] A capacitor-like device is created across the standard sensitizer layer (in analogy to a dielectric in a parallel plate capacitor) through accumulation of negative charges in the $TiO_2$ and positive ones in the cores of type-II QDs. Following this process, a relatively strong dipole is created across the sensitizer layer, inducing a negative shift of the $TiO_2$ energy bands that results in higher $V_{oc}$. The sensitizer layer thus takes two different roles, acting not only as a sensitizer upon light absorption, but also as an "inert" dielectric in the capacitor formed between the type-II QDs and the oxide electrode. It is important to mention that like in a parallel plate capacitor, the PID effect is expected to scale with QD density (charge density) and with standard sensitizer thickness (distance between the two plates). However, this relation breaks down for sufficiently thick sensitizer layers due to the decrease in QD density (less QDs are adsorbed), and the screening effects of charges stored in the standard sensitizer layer.

Figure 1 presents a schematic energy level diagram of the PID cell, also showing its working principles. Upon photoexcitation of a ZnSe/CdS core/shell type-II QD, the electron is injected to the mesoporous $TiO_2$ via the CdS shell and the CdS sensitizer layer, while the hole scavenging by the electrolyte is slowed down due to the CdS shell, leaving the ZnSe core positively charged for a long transient time. In this situation, accumulation of negative charges in the $TiO_2$ (electron conductor) negatively shifts both its conduction and valence bands, while providing higher $V_{oc}$.

In order to understand the role of the photodipole in the QDSSC, the change in band alignment was probed using charge extraction (CE), surface photovoltage (SPV, using Kelvin probe technique), and dark/light current−voltage ($I$−$V$) characteristics.

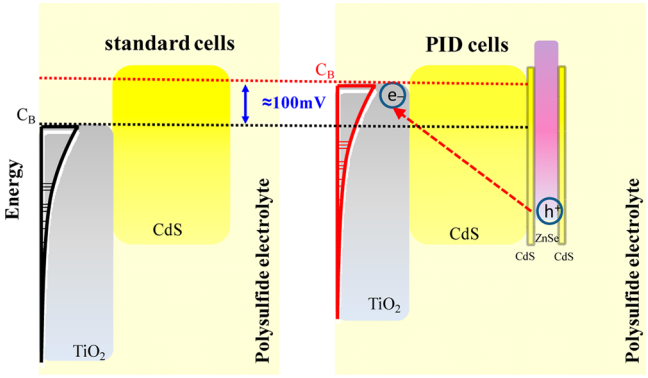


**Figure 1.** Schematic presentation of the photoinduced-dipole (PID) effect. The left side illustrates the standard cell that is composed of a mesoporous-$TiO_2$ and a CdS sensitizer layer. The right side shows how the addition of a ZnSe/CdS type-II QDs monolayer generates a strong dipole that enables a negative shift of the $TiO_2$ energy bands and thus increases the photovoltage upon illumination.

We have systematically studied the PID process in QDSSCs using two different kinds of cells: a reference cell that consists of a mesoporous $TiO_2$ sensitized with common CdS QDs sensitizer layer in various thicknesses (using successive ion layer adsorption and reaction, SILAR), hereafter termed the "standard cell". A cell that is identical to the standard one but in addition contains colloidal type-II ZnSe/CdS QDs adsorbed on the CdS sensitizer layer is termed "PID cell".

Mesoporous (mp) $TiO_2$ was deposited onto a fluorine-doped tin oxide (FTO) conductive glass by the doctor-blade technique using a scotch tape as a spacer. The film was dried and sintered at 500 °C for 30 min to remove the organic materials. The film thickness is measured to be 8 $\mu$m on average. For the CdS growth using the SILAR method, the mesoporous $TiO_2$ film was dipped into the deionized water solution containing 0.1 M $Cd(NO_3)_2{\cdot}4H_2O$ for 1 min to allow $Cd^{2+}$ ions to be adsorbed onto the film. The film was then rinsed with water and immersed into a deionized water solution containing 0.1 M $Na_2S{\cdot}H_2O$ for 1 min to adsorb $S^{2-}$ ions. The adsorbed $S^{2-}$ reacts with $Cd^{2+}$ to form the CdS compound that was anchored onto the $TiO_2$ film to complete one SILAR cycle. Repeating the above procedure increases the loading and thickness of CdS on the $TiO_2$ film. Presynthesized type-II ZnSe/CdS core/shell QDs were deposited directly on the CdS sensitizer by electrophoretic deposition (EPD) from toluene dispersion. Following, all cells were coated with ZnS by SILAR using 0.1 M zinc acetate and 0.1 M of $Na_2S$ (2 cycles). The cells were measured using an aqueous polysulfide redox electrolyte (1 M $Na_2S$, 0.1 M S, and 0.1 M NaOH) and a Pb sheet supported PbS layer as the back electrode.[46]

Figure 2 presents the absorbance spectra of standard (panel a) and PID (panel b) photo anodes for different number of SILAR cycles varying from 2 to 7. As the number of SILAR cycles increases, the CdS sensitizer layer becomes thicker while exhibiting a red-shifted absorbance onset. For the PID cells (Figure 2b), this onset is further red-shifted to about 630 nm due to the absorbance of the type-II QDs. In order to convert the number of CdS SILAR cycles to thickness, standard cells containing 4 and 7 SILAR cycles were probed using FIB (focused ion beam) and HR-TEM (high-resolution transmission electron microscope). The results show (see Figure 3S in the Supporting Information) that the average thickness of 4


dx.doi.org/10.1021/nl402360f | Nano Lett. 2013, 13, 4456−4461

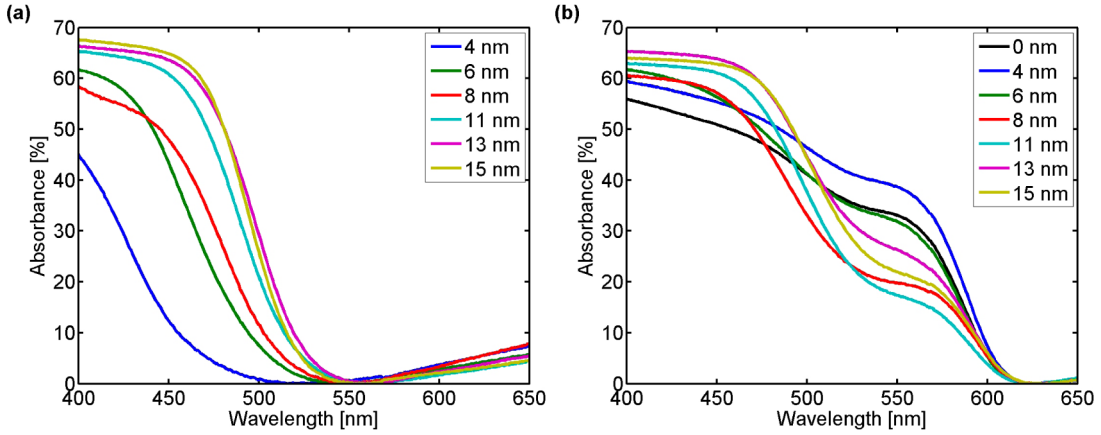


**Figure 2.** Absorbance spectra of standard (a) and PID (b) cells for various CdS sensitizer layer thicknesses grown on mp-$TiO_2$ electrodes. The black curve in panel b represents a cell in which the type-II QDs were deposited directly on the $TiO_2$ surface without a CdS sensitizer layer.

cycles of CdS is 8 nm and that of the 7 cycles is 15 nm, corresponding to about 2 nm/cycle.

In order to understand the effect of the thickness of the CdS sensitizer layer on the extent of the PID effect, photoelectrochemical measurements were conducted. Figure 3 presents the open circuit voltage, measured under 1 sun of simulated illumination (see Figure 4S in the Supporting Information) as a function of CdS sensitizer layer thickness. Clearly, in contrast to the standard cells the $V_{oc}$ values of the PID cells change dramatically with increased thickness of the CdS sensitizer layer. The $V_{oc}$ of a PID cell increases almost by 100 mV going from no CdS sensitizer layer (0 SILAR cycles) to an 8 nm layer (4 SILAR cycles). For thicker layers (5−7 SILAR cycles), the $V_{oc}$ decreases by up to 30 mV from this maximal value. This result can be explained by a combined effect of both PID and dipole charge screening across the CdS sensitizer layer as will be further discussed later in this section.

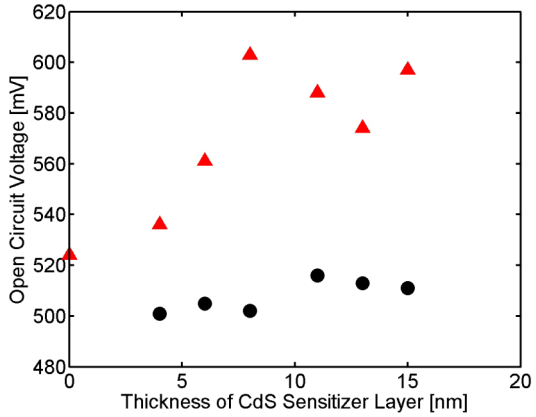


**Figure 3.** Open-circuit voltage ($V_{oc}$) as a function of the CdS sensitizer layer thickness for the standard cells (black dots) and for the PID cells containing the type-II QDs (red triangles). The $V_{oc}$ was measured under 1 sun of simulated illumination (see Figure 4S in the Supporting Information).

Dark $I-V$ measurements were also conducted in order to verify that the additional photovoltage is a result of the dipole that is created under illumination and not due to a constant dipole induced onto the surface of CdS sensitizer layer by adsorbing type-II QDs (see Figure 5S in the Supporting Information). These measurements show no difference between the standard cell and the PID one for the same thickness of the CdS sensitizer layer. In other words, the addition of type-II QDs on the sensitizer layer does not alter either the recombination rates or the electrode energy level alignment in the dark. Consequently the observed voltage changes (Figure 3) are not the result of a constant dipole but rather due to a photo induced process, that is, the PID effect.

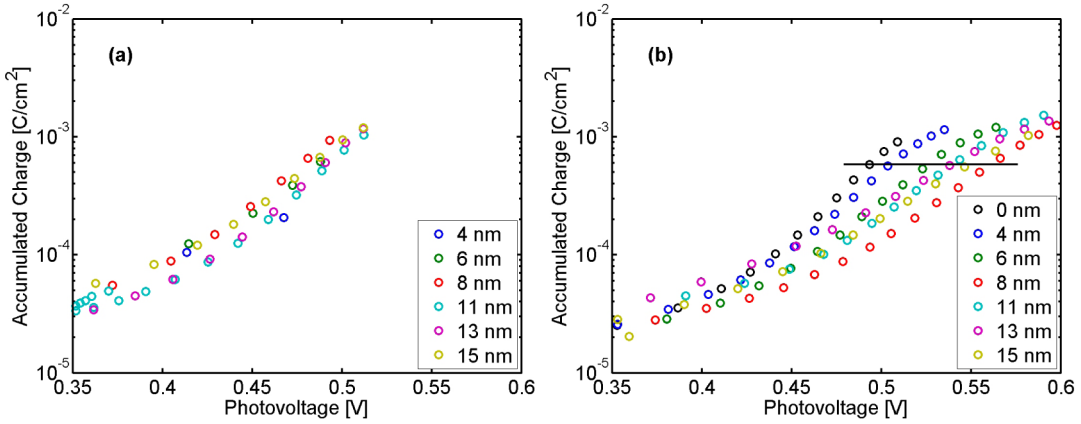


**Figure 4.** Accumulated charge density as a function of the open circuit potential measured for standard (a) and for PID (b) cells with CdS sensitizer layer thicknesses varying from 4 to 15 nm. The results in (a) show an overlap of all the curves, while in (b) there is a clear shift of the curves indicating shifts of the $TiO_2$ energy bands due to the PID effect.


dx.doi.org/10.1021/nl402360f | *Nano Lett.* 2013, 13, 4456−4461

Charge extraction (CE) was measured in order to retrieve the extent of energy band shifts occurring due to the PID effect. In this measurement, the cells are subject to a variable light at open circuit conditions. When a steady $V_{oc}$ is reached at specific illumination intensity, the cell is short circuited via a known resistor to collect the accumulated charge within the electrode. A plot of charge density as a function of the photovoltage can be seen in Figure 4. For the standard cells (Figure 4a), all curves, representing different thicknesses of CdS sensitizer layer, are overlapping. This means that the position of the $TiO_2$ energy bands is constant for all these cells. In contrast, the curves that were obtained from the PID cells in Figure 4b clearly show a photo-induced dipole effect that is pointing to the surface of the $TiO_2$. As the sensitizer layer becomes thicker, the accumulated charge for the same $V_{oc}$ decreases, meaning that the $TiO_2$ energy bands were negatively shifted due to the increase in the dipole moment. As already mentioned above, for CdS sensitizer layers thicker than 8 nm (5−7 SILAR cycles), the PID effect is probably screened by accumulated charges inside the CdS sensitizer layer and one can observe a positive shift in the $TiO_2$ energy bands, causing the reduction in the measured $V_{oc}$. Therefore, we can conclude that at thin CdS sensitizer layer the PID effect is the dominant one. In contrast, at thicker CdS sensitizer layer (more than 8 nm), electrons need to diffuse a longer path in order to reach the $TiO_2$, resulting in negative charge accumulation in the sensitizer layer (CdS). This leads to screening of the PID (decrease in the dipole moment) and consequently to the smaller increase in the $V_{oc}$.

In addition to the CE results presented in Figure 4, which show an increase in the dipole moment (and as a result in $V_{oc}$) as the CdS sensitizer layer becomes thicker, there is also a meaning to the rate of change in the $V_{oc}$ with the change in the illumination intensity for each PID cell. These rate changes were obtained for all cells by the following manner: for each PID cell, at any given charge density, we have calculated the $V_{oc}$ difference compared to a PID cell with no CdS sensitizer layer (e.g., along the black solid line in Figure 4b). Figure 5 shows

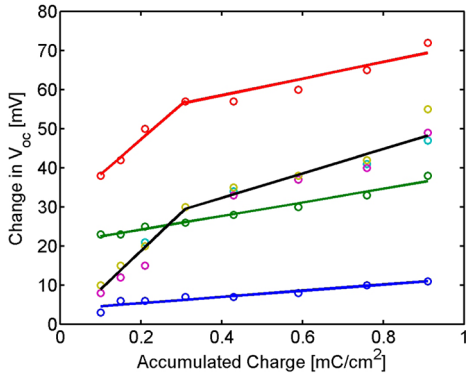


**Figure 5.** Change in the $V_{oc}$ of PID cells compared to a PID cell with no CdS sensitizer layer (type-II QDs deposited directly on the $TiO_2$ surface) as a function of the accumulated charge density (extracted from Figure 4b). The trend lines are linear fittings to the data points shown as circles. Color caption: blue, 4 nm; green, 6 nm; red, 8 nm; cyan, 11 nm; magenta, 13 nm; yellow, 15 nm. The black trend line represents the average slope for 11, 13, and 15 nm cells. The slopes of the cells with 8, 11, 13, and 15 nm CdS layer were divided into two regions, below and above 0.3 mC/cm$^2$, which represents the dominance transition point between the PID effect and the dipole screening phenomenon.

these results, derived from Figure 4b (note that we flip the $X$ and $Y$ axes). The rate of $V_{oc}$ change (the slope in Figure 5) increases significantly when the CdS sensitizer layer is thickened from 4 to 6 nm, indicating that a larger PID is formed between holes in the type-II ZnSe cores and electrons in the $TiO_2$. However, when the CdS sensitizer layer gets even thicker (8−15 nm), we observe two different slopes. At low light intensities, the slope is much steeper than that of the 6 nm layer, in accordance with the PID effect. However, at higher accumulated charge densities (0.3 mC/cm$^2$), the slope drops to lower values indicating the dominance of the screening effect which cancels part of the PID. These observations highlight the relative complexity of our system, where the two roles of the CdS layer, acting both as sensitizer and as the "inert" capacitive layer are contradicting, particularly for thick layers and high excitation fluences. Indeed, this reflects that under operating conditions, while the PID effect is clearly present, analysis of its relative magnitude must be supported by an independent measurement, as follows.

An independent observation of the PID effect was obtained using the surface photovoltage (SPV) technique. The measurements were performed using a commercial Kelvin probe (Besocke Delta-Phi, Julich, Germany), as part of a home-built setup, inside a glovebox. The schematic representation of the setup can be seen in Figure 6a. The setup consists of two electrically connected electrodes that form a parallel plate capacitor. The first is a vibrating gold grid, which is the reference electrode, and the second one is the sample; in this case, it is a photoanode half cell without the electrolyte and the PbS counter electrode. The capacitor is either measured in dark or illuminated with a tungsten-halogen lamp with varying intensities through an infrared (IR) absorbing filter. The light intensities that were used are 10, 30, 56, and 94 mW/cm$^2$ and were obtained by changing the voltage falling on the lamp using the Variac autotransformer. All the setup elements, except the autotransformer, were put in a Faraday cage to minimize electrical interference from external sources.

This configuration allows for determination of work function difference between the two materials (electrodes) forming the two sides of the parallel plate capacitor. More details about this technique can be found in the Supporting Information.

In our system, because holes are confined to the ZnSe cores in the PID cell for a long time (in the absence of an electrolyte to harvest them), we expect for a maximal obtainable dipole effect for a given thickness of a CdS sensitizer layer. This dipole is expected to contribute more to the SPV signal as compared to the standard cell because of a larger change in the surface potential. The obtained results are presented in Figure 6b,c for the standard and the PID cell, respectively. The SPV values of both cells were shifted for simplicity, such that the contact potential difference (CPD) values (dark) are at zero.

From Figure 6b,c, it can be seen that the voltage difference (SPV) for the standard cell with 8 nm CdS sensitizer layer is about 175 mV, whereas for the PID cell with the same CdS sensitizer layer thickness, is 315 mV under light power density of 56 mW/cm$^2$. This result implies that the extractable photovoltage from the PID cell is higher by ∼140 mV relative to that from the standard cell. In order to estimate the contribution of the photodipole to the overall difference in the SPV between these two cells (140 mV), extra absorbed photons by the PID cell should be taken into consideration. The PID cell absorbs 5 times more photons relative to the standard cell under the illumination used in the SPV setup due to the type-II


dx.doi.org/10.1021/nl402360f | Nano Lett. 2013, 13, 4456−4461

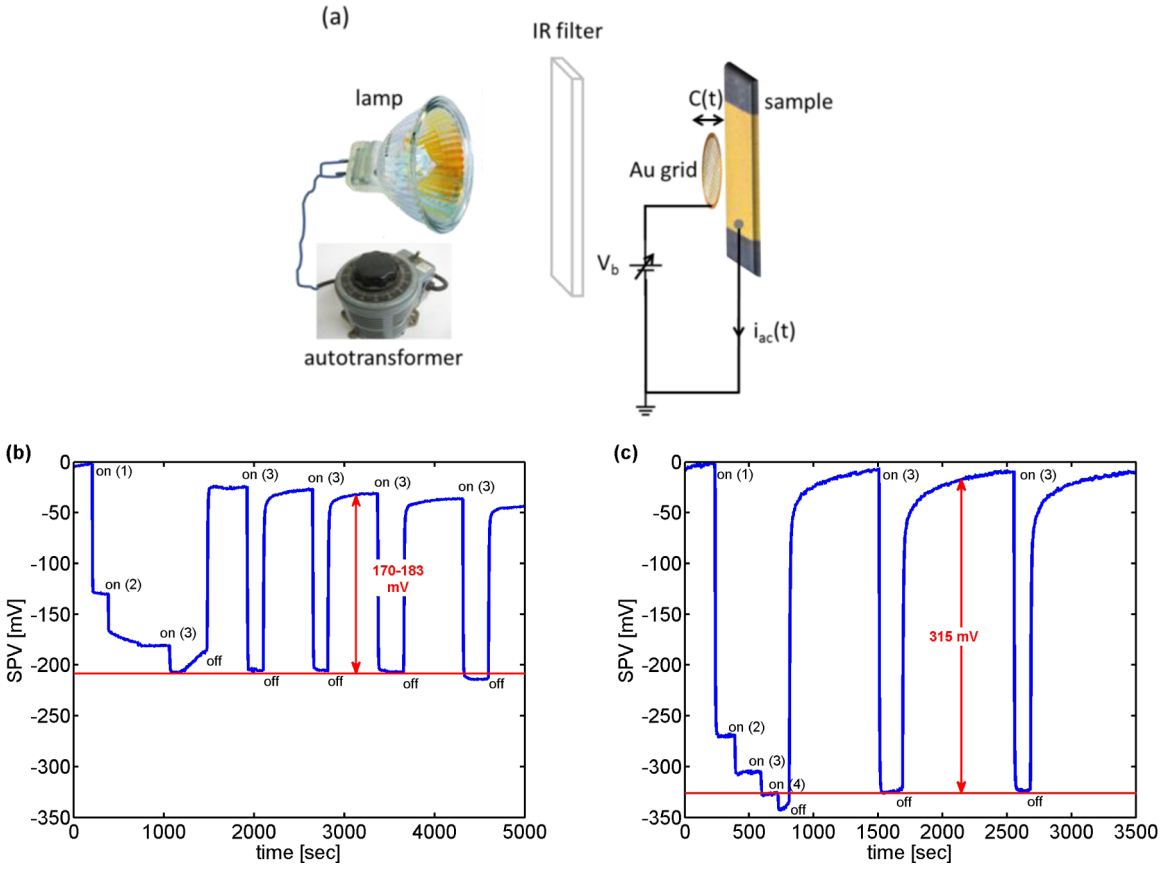


**Figure 6.** (a) Schematic representation of the SPV setup. (b,c) The SPV as a function of the light illumination intensity for the standard and the PID cell, respectively, both with 8 nm of CdS sensitizer layer (4 SILAR cycles). "Off" stands for the dark and "on" for the light, while (1) 10 mW/cm$^2$; (2) 30 mW/cm$^2$; (3) 56 mW/cm$^2$; and (4) 94 mW/cm$^2$. The light modulation between the dark and the 56 mW/cm$^2$ (on (3)) was performed for both cells and the difference in voltage between these two states is shown by red arrows.

QDs adsorbed onto it (data not shown). From Figure 4a, it can be calculated that a 10-fold increment in charge density, increases the extractable photovoltage by ∼100 mV, thus 5 times increase in the absorbed photons will increase the photovoltage by 70 mV, under the assumption that all the absorbed photons have equal probability to be converted to an electrical charge. It means that the net contribution to the photovoltage due to the PID effect is ∼70 mV for the 8 nm CdS sensitizer layer. Notably, very similar values for the voltage shift were obtained from the two completely different techniques described above.

To conclude, we present a new phenomenon in QDSSC, which we term the photoinduced dipole (PID) effect. In these types of cells, the adsorbed type-II ZnSe/CdS core/shell QDs on the CdS sensitizer layer have two functions. First, they are responsible for the PID effect that originates from the efficient separation of charges across the photoactive electrode (accumulation of negative charges in the $TiO_2$ and positive charges in the ZnSe cores) creating a dipole moment. This PID negatively shifts the energy bands of $TiO_2$, while significantly increasing the solar cell $V_{oc}$. Second, these type-II QDs are able to absorb solar light and inject photoexcited electrons to the $TiO_2$ to improve the photocurrent of the cell. We have shown that the PID can increase the $V_{oc}$ by ∼80 mV, a value that was obtained using two different measurement techniques. This voltage increase partially compensates for the overpotential losses associated with the difference between the conduction band of the CdS and that of the $TiO_2$, while not affecting the rates of electron injection. Potentially, even higher photovoltages can be obtained if the cell's accumulated charge density will be increased by increasing the loading of the type-II QDs inside the electrode. Understanding the PID physical properties, as well as its limitations, is currently under investigation in our laboratory. Moreover, due to the flexibility of the PID concept this work introduces a new design strategy toward the development of additional kinds of high voltage PV cells such as solid state QDSSCs, organic solar cells (OPV), Schottky junction cells, and perovskite based solar cells.[31,47−49]

## ■ ASSOCIATED CONTENT

### Supporting Information

Additional information: chemicals, synthesis of QDs, TEM image of QDs, film preparation, TEM image of the films, photo electrochemical measurements (I-*V* light and I-*V* dark) and SPV measurements. This material is available free of charge via the Internet at http://pubs.acs.org.

## ■ AUTHOR INFORMATION

### Corresponding Author

*E-mail: arie.zaban@biu.ac.il; dan.oron@weizmann.ac.il.

### Author Contributions

§S.B and S.I. contributed equally.

### Notes

The authors declare no competing financial interest.

## ■ ACKNOWLEDGMENTS

A.Z. thanks the Israel Strategic Alternative Energy Foundation (I-SAEF), Israel, for the financial support. S.B. is grateful for the support of the Adams Fellowship Program of the Israel Academy of Sciences and Humanities. D.O. is the incumbent of the Recanati career development chair in energy researches and acknowledges financial support from the Leona M. and Harry B. charitable trust.

## ■ REFERENCES

(1) Dittrich, T.; Belaidi, A.; Ennaoui, A. *Sol. Energy Mater. Sol. Cells* **2011**, *95*, 1527−1536.
(2) Hodes, G. *J. Phys. Chem. C* **2008**, *112*, 17778−17787.
(3) Kamat, P. V.; Tvrdy, K.; Baker, D. R.; Radich, J. G. *Chem. Rev.* **2010**, *110*, 6664−6688.
(4) Ruhle, S.; Shalom, M.; Zaban, A. *ChemPhysChem* **2010**, *11*, 2290−2304.
(5) Barkhouse, D. A. R.; Debnath, R.; Kramer, I. J.; Zhitomirsky, D.; Pattantyus-Abraham, A. G.; Levina, L.; Etgar, L.; Gratzel, M.; Sargent, E. H. *Adv. Mater.* **2011**, *23*, 3134−3138.
(6) Shalom, M.; Dor, S.; Ruhle, S.; Grinis, L.; Zaban, A. *J. Phys. Chem. C* **2009**, *113*, 3895−3898.
(7) Diguna, L. J.; Shen, Q.; Kobayashi, J.; Toyoda, T. *Appl. Phys. Lett.* **2007**, *91*, 023116−023119.
(8) Gur, I.; Fromer, N. A.; Geier, M. L.; Alivisatos, A. P. *Science* **2005**, *310*, 462−465.
(9) Hachiya, S.; Shen, Q.; Toyoda, T. *J. Appl. Phys.* **2012**, 111104315−104319.
(10) Nozik, A. J. *Nano Lett.* **2010**, *10*, 2735−2741.
(11) Salant, A.; Shalom, M.; Hod, I.; Faust, A.; Zaban, A.; Banin, U. *ACS Nano* **2010**, *4*, 5962−5968.
(12) Zaban, A.; Micic, O. I.; Gregg, B. A.; Nozik, A. J. *Langmuir* **1998**, *14*, 3153−3156.
(13) Kamat, P. V. *J. Phys. Chem. C* **2008**, *112*, 18737−18753.
(14) Guijarro, N.; Lana-Villarreal, T.; Lutz, T.; Haque, S. A.; Gomez, R. *J. Phys. Chem. Lett.* **2012**, *3*, 3367−3372.
(15) Buhbut, S.; Itzhakov, S.; Oron, D.; Zaban, A. *J. Phys. Chem. Lett.* **2011**, *2*, 1917−1924.
(16) Buhbut, S.; Itzhakov, S.; Tauber, E.; Shalom, M.; Hod, I.; Geiger, T.; Garini, Y.; Oron, D.; Zaban, A. *ACS Nano* **2010**, *4*, 1293−1298.
(17) Itzhakov, S.; Buhbut, S.; Tauber, E.; Geiger, T.; Zaban, A.; Oron, D. *Adv. Energy Mater.* **2011**, *1*, 626−633.
(18) Han, H.; Sudhagar, P.; Song, T.; Jeon, Y.; Mora-Sero, I.; Fabregat-Santiago, F.; Bisquert, J.; Kang, Y. S.; Paik, U. *Chem. Commun.* **2013**, *49*, 2810−2812.
(19) Oregan, B.; Gratzel, M. *Nature* **1991**, *353*, 737−740.
(20) Mora-Sero, I.; Bisquert, J. *J. Phys. Chem. Lett.* **2010**, *1*, 3046−3052.
(21) Kamat, P. V. *J. Phys. Chem. Lett.* **2013**, *4*, 908−918.
(22) Santra, P. K.; Kamat, P. V. *J. Am. Chem. Soc.* **2012**, *134*, 2508−2511.
(23) Lee, J.-W.; Son, D.-Y.; Ahn, T. K.; Shin, H.-W.; Kim, I. Y.; Hwang, S.-J.; Ko, M. J.; Sul, S.; Han, H.; Park, N.-G. *Sci. Rep.* **2013**, DOI: 10.1038/srep01050.
(24) Im, S. H.; Lim, C. S.; Chang, J. A.; Lee, Y. H.; Maiti, N.; Kim, H. J.; Nazeeruddin, M. K.; Gratzel, M.; Seok, S. I. *Nano Lett.* **2011**, *11*, 4789−4793.
(25) de la Fuente, M. S.; Sanchez, R. S.; Gonzalez-Pedro, V.; Boix, P. P.; Mhaisalkar, S. G.; Rincon, M. E.; Bisquert, J.; Mora-Sero, I. *J. Phys. Chem. Lett.* **2013**, *4*, 1519−1525.
(26) Fan, J. D.; Hao, Y.; Cabot, A.; Johansson, E. M. J.; Boschloo, G.; Hagfeldt, A. *ACS Appl. Mater. Interfaces* **2013**, *5*, 1902−1906.
(27) Lim, C. S.; Im, S. H.; Rhee, J. H.; Lee, Y. H.; Kim, H. J.; Maiti, N.; Kang, Y.; Chang, J. A.; Nazeeruddin, M. K.; Gratzel, M.; Seok, S. I. *J. Mater. Chem.* **2012**, *22*, 1107−1111.
(28) Fantacci, S.; De Angelis, F.; Nazeeruddin, M. K.; Graetzel, M. *J. Phys. Chem. C* **2011**, *115*, 23126−23133.
(29) Chang, J. A.; Im, S. H.; Lee, Y. H.; Kim, H. J.; Lim, C. S.; Heo, J. H.; Seok, S. I. *Nano Lett.* **2012**, *12*, 1863−1867.
(30) Chang, J. A.; Rhee, J. H.; Im, S. H.; Lee, Y. H.; Kim, H. J.; Seok, S. I.; Nazeeruddin, M. K.; Gratzel, M. *Nano Lett.* **2010**, *10*, 2609−2612.
(31) Baikie, T.; Fang, Y. N.; Kadro, J. M.; Schreyer, M.; Wei, F. X.; Mhaisalkar, S. G.; Graetzel, M.; White, T. J. *J. Mater. Chem. A* **2013**, *1*, 5628−5641.
(32) Cohen, R.; Kronik, L.; Shanzer, A.; Cahen, D.; Liu, A.; Rosenwaks, Y.; Lorenz, J. K.; Ellis, A. B. *J. Am. Chem. Soc.* **1999**, *121*, 10545−10553.
(33) Salomon, A.; Berkovich, D.; Cahen, D. *Appl. Phys. Lett.* **2003**, *82*, 1051−1053.
(34) Selzer, Y.; Cahen, D. *Adv. Mater.* **2001**, *13*, 508−511.
(35) Visoly-Fisher, I.; Sitt, A.; Wahab, M.; Cahen, D. *ChemPhysChem.* **2005**, *6*, 277−285.
(36) Schlichthorl, G.; Huang, S. Y.; Sprague, J.; Frank, A. J. *J. Phys. Chem. B* **1997**, *101*, 8141−8155.
(37) Ruhle, S.; Greenshtein, M.; Chen, S. G.; Merson, A.; Pizem, H.; Sukenik, C. S.; Cahen, D.; Zaban, A. *J. Phys. Chem. B* **2005**, *109*, 18907−18913.
(38) Hod, I.; Tachan, Z.; Shalom, M.; Zaban, A. *Phys. Chem. Chem. Phys.* **2013**, *15*, 6339−6343.
(39) Shalom, M.; Ruhle, S.; Hod, I.; Yahav, S.; Zaban, A. *J. Am. Chem. Soc.* **2009**, *131*, 9876−9877.
(40) Barea, E. M.; Shalom, M.; Gimenez, S.; Hod, I.; Mora-Sero, I.; Zaban, A.; Bisquert, J. *J. Am. Chem. Soc.* **2010**, *132*, 6834−6839.
(41) Hod, I.; Gonzalez-Pedro, V.; Tachan, Z.; Fabregat-Santiago, F.; Mora-Sero, I.; Bisquert, J.; Zaban, A. *J. Phys. Chem. Lett.* **2011**, *2*, 3032−3035.
(42) Shalom, M.; Tachan, Z.; Bouhadana, Y.; Barad, H.-N.; Zaban, A. *J. Phys. Chem. Lett.* **2011**, *2*, 1998−2003.
(43) Shalom, M.; Buhbut, S.; Tirosh, S.; Zaban, A. *J. Phys. Chem. Lett.* **2012**, *3*, 2436−2441.
(44) Ivanov, S. A.; Piryatinski, A.; Nanda, J.; Tretiak, S.; Zavadil, K. R.; Wallace, W. O.; Werder, D.; Klimov, V. I. *J. Am. Chem. Soc.* **2007**, *129*, 11708−11719.
(45) Itzhakov, S.; Shen, H.; Buhbut, S.; Lin, H.; Oron, D. *J. Phys. Chem. C.* **2012**, DOI: 10.1021/jp312190x.
(46) Tachan, Z.; Shalom, M.; Hod, I.; Ruehle, S.; Tirosh, S.; Zaban, A. *J. Phys. Chem. C* **2011**, *115*, 6162−6166.
(47) Kim, H.-S.; Lee, C.-R.; Im, J.-H.; Lee, K.-B.; Moehl, T.; Marchioro, A.; Moon, S.-J.; Humphry-Baker, R.; Yum, J.-H.; Moser, J. E.; Graetzel, M.; Park, N.-G. *Sci. Rep.* **2012**, DOI: 10.1038/srep00591.
(48) Lee, M. M.; Teuscher, J.; Miyasaka, T.; Murakami, T. N.; Snaith, H. J. *Science* **2012**, *338*, 643−647.
(49) Im, J.-H.; Lee, C.-R.; Lee, J.-W.; Park, S.-W.; Park, N.-G. *Nanoscale* **2011**, *3*, 4088−4093.